

Extended Skyrme interactions for nuclear matter, finite nuclei and neutron stars

Zhen Zhang¹ and Lie-Wen Chen^{*1,2}

¹*Department of Physics and Astronomy and Shanghai Key Laboratory for Particle Physics and Cosmology, Shanghai Jiao Tong University, Shanghai 200240, China*

²*Center of Theoretical Nuclear Physics, National Laboratory of Heavy Ion Accelerator, Lanzhou 730000, China*
(Dated: October 23, 2015)

Recent progress in theory, experiment and observation challenges the mean field models using the conventional Skyrme interaction, suggesting that the extension of the conventional Skyrme interaction is necessary. In this work, we construct three Skyrme interaction parameter sets, namely, eMSL07, eMSL08 and eMSL09, based on an extended Skyrme interaction which includes additional momentum and density dependent two-body forces to effectively simulate the momentum dependence of the three-body force. The three new interactions can well reproduce both the ground-state properties and isoscalar giant monopole resonance energy of finite nuclei, nicely conform to the current knowledge on the equation of state of asymmetric nuclear matter around and below saturation density ρ_0 , eliminate the notorious unphysical instabilities of symmetric nuclear matter and pure neutron matter at densities up to about $7.5\rho_0$, and simultaneously support heavier neutron stars with mass larger than two times solar mass. The new family of the extended Skyrme interactions can thus provide a unified description for the properties of asymmetric nuclear matter from sub- to supra-saturation densities in large region of isospin values and are appropriate for the study of nuclear matter, finite nuclei and neutron stars.

PACS numbers: 21.65.Ef, 21.30.Fe, 21.60.Jz, 26.60.Dd

I. INTRODUCTION

The exact knowledge on infinite nuclear matter, which is intimately related to the in-medium effective nuclear interactions, is of fundamental importance in nuclear physics and astrophysics [1–4]. Especially, the equation of state (EOS) of isospin asymmetric nuclear matter is the main ingredient in the study of neutron stars. In principle, the nuclear matter EOS can be obtained from various microscopic many-body approaches, e.g., the nonrelativistic and relativistic Brueckner-Hartree-Fock (BHF) method [5–7], the variational many-body approach [8, 9], quantum Monte Carlo (QMC) method [10–12] and chiral effective field theory (ChEFT) [13, 14], using realistic nuclear forces. However, due to the poorly known many-body interactions and the limitations in the techniques for solving the nuclear many-body problem, accurate determination of properties of nuclear matter around and beyond saturation density ρ_0 is still an open challenge for microscopic many-body theory. Another different perspective is the mean field model using phenomenological nuclear effective interactions with several parameters adjusted by fitting experimental data [15]. Among various phenomenological interactions, the nonrelativistic zero-range and density-dependent Skyrme-type effective nucleon-nucleon interactions perhaps are the most widely used. Proposed by Skyrme in the 1950s [16] and firstly applied in the study of finite nuclei in Hartree-Fock (HF) calculations by Brink and Vautherin in 1970s [17], the Skyrme interaction enormously simplifies the calcu-

lations with its zero-range form and has been very successfully used to describe the mass, charge radii and excited states of finite nuclei as well as the EOS of nuclear matter around ρ_0 . Moreover, extrapolation to high-density region based on the Skyrme-Hartree-Fock (SHF) model provides an important approach to investigate the properties of dense nuclear matter and the relevant astrophysics problems, especially the properties of neutron stars.

Since 1970s, a lot of work has been devoted to improving the Skyrme interaction to better reproduce the experimental data or describe different physical objects. Recently, much attention has been given to the problem of searching for effective interactions or energy density functionals (EDFs) which could simultaneously reproduce the properties of nuclear matter and finite nuclei, and at the same time be applicable for the study of neutron stars [15, 18–20]. This problem is of particular interest as two very heavy neutron stars with mass of two times solar mass ($2M_\odot$) have been observed recently [21, 22], which requires the pressure of high-density nuclear matter should be large enough to support such massive neutron stars against the strong gravity. This requirement is a big challenge for many theoretical models and indeed rules out essentially all the soft nuclear matter EOSs. Given the EOS of symmetric nuclear matter has been relatively well constrained even up to about $5\rho_0$ by analyzing the experimental data on giant resonances of finite nuclei [23–25] as well as the collective flows and kaon production in heavy-ion collisions [26–28], a model predicting $2M_\odot$ neutron stars generally rules out a softer symmetry energy at high densities. It should be pointed out that some new physical mechanisms, such as non-Newtonian gravity [29–32], may support $2M_\odot$ neutron

*Corresponding author (email: lwchen@sjtu.edu.cn)

stars with a soft symmetry energy. In the present work we shall focus on the standard nuclear physics without considering these new physics.

During the last decade, considerable progress in determining the symmetry energy or neutron matter EOS at subsaturation densities has been made, both theoretically and experimentally. Indeed, it has been well established that the binding energy of finite nuclei can put rather stringent constraints on the symmetry energy at a subsaturation density $\rho \approx (2/3)\rho_0$ [33–38]. For the symmetry energy at a even lower density $\rho \approx \rho_0/3$, it has been shown recently [39] that the measurement of the electric dipole polarizability in ^{208}Pb can give a quite accurate constraint and the result is in very good agreement with the constraints from SHF analyses of isobaric analog states and neutron skin data [36] as well as the transport model analyses of mid-peripheral heavy-ion collisions of Sn isotopes [40]. For pure neutron matter, very similarly, the binding energy per neutron around subsaturation densities $(2/3)\rho_0$ and $\rho_0/3$ has been constrained by analyzing the ground-state properties of doubly magic nuclei [38] and the electric dipole polarizability in ^{208}Pb [39]. In particular, the calculations based on the microscopic ChEFT [14] and QMC calculations [10–12] have provided very useful information on the EOS of pure neutron matter, especially at subsaturation densities. These theoretical and experimental constraints consistently favor a relatively soft symmetry energy or EOS of asymmetric nuclear matter, at least at subaturation densities around $(2/3)\rho_0$. The symmetry energy softer at subsaturation densities favored by experimental constraints and theoretical predictions but stiffer at higher densities favored by the observation of $2M_\odot$ neutron stars challenges the SHF model with the conventional Skyrme interactions. For example, the Skyrme interaction TOVmin [19], which is built by fitting properties of both finite nuclei and neutron stars, can successfully support $2M_\odot$ neutron stars but predict a neutron matter EOS significantly deviating from ChEFT calculations [14] and the constraint extracted from analyzing the electric dipole polarizability in ^{208}Pb [39] at densities below about $0.5\rho_0$.

Furthermore, it is well known that a notorious shortcoming of the conventional standard Skyrme interactions is that they predict various instabilities of nuclear matter around saturation density or at supra-saturation densities, which in principle hinders the application of the Skyrme interactions in the study of dense nuclear matter as well as neutron stars. For instance, whereas most of the conventional standard Skyrme interactions predict spin or spin-isospin polarization in the density region of ρ_0 – $3.5\rho_0$ [18, 41], the calculations based on the microscopic many-body theory using realistic nuclear forces, such as relativistic and nonrelativistic BHF approach [42, 43], the QMC method [44], the ChEFT method [45], and the lowest order constrained variational approach [46], predict no such instabilities at densities up to substantially high densities. To solve this problem, Margueron and Sagawa proposed an extended form of the

Skyrme interaction with additional density-dependent terms [47], while Chamel *et al.* introduced momentum and density dependent terms which are density-dependent generalizations of the usual t_1 and t_2 terms in the conventional standard Skyrme interaction [48]. In particular, in Ref. [49], Chamel and Goriely find that the spin and spin-isospin instabilities can be removed by omitting the time-odd terms in $(\mathbf{s}_n + \mathbf{s}_p) \times (\mathbf{T}_n + \mathbf{T}_p)$ and $(\mathbf{s}_n - \mathbf{s}_p) \times (\mathbf{T}_n - \mathbf{T}_p)$, namely setting $C_0^T = C_1^T = 0$ in the notation of Ref. [50]. Nevertheless, this imposition yields unrealistic Landau parameters in spin and spin-isospin channels and in principle the associated time-even terms in J^2 and J_q^2 also should be dropped for self-consistence.

In Ref. [18], Dutre *et al.* find that, of 240 standard Skyrme interactions, only 6 satisfy all eleven constraints on the properties of nuclear matter selected therein. Nevertheless, we would like to point out that all the 6 Skyrme interactions predict spin or spin-isospin instabilities below $3\rho_0$ and fail to produce $2M_\odot$ neutron stars. In the present work, we show that the above problems existed in the conventional standard Skyrme interactions can be addressed within the framework of an extended Skyrme interaction [48, 51–56] which includes additional terms to effectively simulate the momentum dependence of the three-body force. Our purpose here is to construct parameter sets of the extended Skyrme interactions that can well reproduce the properties of finite nuclei, conform to the most recent constraints on nuclear matter, especially the EOS of asymmetric nuclear matter at subsaturation densities, and eliminate the anomalous instabilities of nuclear matter in the density region encountered in neutron stars. Furthermore, we find that the new family of the extended Skyrme interactions can successfully support $2M_\odot$ neutron stars and predict reasonable stellar radii. The new extended Skyrme interactions thus provide a universal approach to describe nuclear matter, finite nuclei and neutron stars.

The paper is organized as follows. In Sec. II, we introduce the form of the extended Skyrme interaction and the energy density functional adopted in this work. In Sec. III, the experimental data and constraints used in our fitting are presented. The parameter sets of three new extended Skyrme interactions and the corresponding results are exhibited in Sec. IV. Finally, we summarize our conclusions in Sec. V. Appendix A gives the expressions for several macroscopic quantities in the extended SHF model and Appendix B presents the analytical relations between the chosen macroscopic quantities and the microscopic Skyrme parameters.

II. MODELS AND METHODS

A. Extended Skyrme-Hartree-Fock model

In the conventional SHF model, nucleons generally interact with each other through the so-called standard

Skyrme interaction (see, e.g., Ref. [57])

$$\begin{aligned}
v(\mathbf{r}_1, \mathbf{r}_2) = & t_0(1 + x_0 P_\sigma) \delta(\mathbf{r}_1 - \mathbf{r}_2) \\
& + \frac{1}{2} t_1(1 + x_1 P_\sigma) [\mathbf{k}'^2 \delta(\mathbf{r}_1 - \mathbf{r}_2) + \text{c.c.}] \\
& + t_2(1 + x_2 P_\sigma) \mathbf{k}' \cdot \delta(\mathbf{r}_1 - \mathbf{r}_2) \mathbf{k} \\
& + \frac{1}{6} t_3(1 + x_3 P_\sigma) \rho^\alpha \left(\frac{\mathbf{r}_1 + \mathbf{r}_2}{2} \right) \delta(\mathbf{r}_1 - \mathbf{r}_2) \\
& + i W_0 (\boldsymbol{\sigma}_1 + \boldsymbol{\sigma}_2) \cdot [\mathbf{k}' \times \delta(\mathbf{r}_1 - \mathbf{r}_2) \mathbf{k}], \quad (1)
\end{aligned}$$

where $\boldsymbol{\sigma}_i$ is the Pauli spin operator, P_σ is the spin-exchange operator, $\mathbf{k} = -i(\nabla_1 - \nabla_2)/2$ is the relative momentum operator, and \mathbf{k}' is the conjugate operator of \mathbf{k} acting on the left.

In the present work, to take account of the momentum dependence of the three body interaction, we use the extended Skyrme interaction with the following additional zero-range density- and momentum-dependent terms [48, 51–56]

$$\begin{aligned}
& + \frac{1}{2} t_4(1 + x_4 P_\sigma) \left[\mathbf{k}'^2 \rho^\beta \left(\frac{\mathbf{r}_1 + \mathbf{r}_2}{2} \right) \delta(\mathbf{r}_1 - \mathbf{r}_2) + \text{c.c.} \right] \\
& + t_5(1 + x_5 P_\sigma) \mathbf{k}' \cdot \rho^\gamma \left(\frac{\mathbf{r}_1 + \mathbf{r}_2}{2} \right) \delta(\mathbf{r}_1 - \mathbf{r}_2) \mathbf{k}, \quad (2)
\end{aligned}$$

which are just the density dependent generalization of the t_1 and t_2 terms in Eq. (1). For simplicity, β and γ are set to be unit in the present work, just like the form used in Ref. [52–54]. It should be noted that in HF calculations the zero-range momentum dependent three-body force is equivalent to a momentum and density dependent two-body force for spin-saturated systems, and the original values of β and γ are just unit [58]. Therefore, there are thirteen Skyrme parameters $t_0 \sim t_5$, $x_0 \sim x_5$ and α in the present extended Skyrme interaction.

In Hartree-Fock approach with the extended Skyrme interaction, the total energy density of a nucleus can be expressed as

$$\mathcal{H} = \mathcal{K} + \mathcal{H}_0 + \mathcal{H}_3 + \mathcal{H}_{\text{eff}} + \mathcal{H}_{\text{fin}} + \mathcal{H}_{\text{SO}} + \mathcal{H}_{\text{sg}} + \mathcal{H}_{\text{Coul}}, \quad (3)$$

where $\mathcal{K} = \frac{\hbar^2}{2m} \tau$ is the kinetic-energy term and \mathcal{H}_0 , \mathcal{H}_3 , \mathcal{H}_{eff} , \mathcal{H}_{fin} , \mathcal{H}_{SO} , \mathcal{H}_{sg} are given by

$$\mathcal{H}_0 = \frac{1}{4} t_0 [(2 + x_0) \rho^2 - (2x_0 + 1)(\rho_n^2 + \rho_p^2)], \quad (4)$$

$$\mathcal{H}_3 = \frac{1}{24} t_3 \rho^\alpha [(2 + x_3) \rho^2 - (2x_3 + 1)(\rho_n^2 + \rho_p^2)], \quad (5)$$

$$\begin{aligned}
\mathcal{H}_{\text{eff}} = & \frac{1}{8} [t_1(2 + x_1) + t_2(2 + x_2)] \rho \tau \\
& - \frac{1}{8} [t_1(2x_1 + 1) - t_2(2x_2 + 1)] (\rho_n \tau_n + \rho_p \tau_p), \\
& + \frac{1}{8} [t_4(2 + x_4) \rho^\beta + t_5(2 + x_5) \rho^\gamma] \rho \tau \\
& - \frac{1}{8} [t_4(2x_4 + 1) \rho^\beta - t_5(2x_5 + 1) \rho^\gamma] (\rho_n \tau_n + \rho_p \tau_p), \quad (6)
\end{aligned}$$

$$\begin{aligned}
\mathcal{H}_{\text{fin}} = & \frac{1}{32} [3t_1(2 + x_1) - t_2(2 + x_2)] (\nabla \rho)^2 \\
& - \frac{1}{32} [3t_1(2x_1 + 1) + t_2(2x_2 + 1)] \sum_{q=n,p} (\nabla \rho_q)^2 \\
& + \frac{1}{32} [(2\beta + 3)t_4(2 + x_4) \rho^\beta - t_5(2 + x_5) \rho^\gamma] (\nabla \rho)^2 \\
& - \frac{1}{32} [3t_4(2x_4 + 1) \rho^\beta + t_5(2x_5 + 1) \rho^\gamma] \sum_{q=n,p} (\nabla \rho_q)^2 \\
& - \frac{\beta}{16} t_4(2x_4 + 1) \rho^{\beta-1} \nabla \rho \sum_{q=n,p} \rho_q \nabla \rho_q \quad (7)
\end{aligned}$$

$$\mathcal{H}_{\text{SO}} = \frac{1}{2} W_0 [J \cdot \nabla \rho + J_n \nabla \rho_n + J_p \nabla \rho_p] \quad (8)$$

$$\begin{aligned}
\mathcal{H}_{\text{sg}} = & -\frac{1}{16} (t_1 x_1 + t_2 x_2) J^2 + \frac{1}{16} (t_1 - t_2) \sum_{q=n,p} J_q^2 \\
& - \frac{1}{16} (t_4 x_4 \rho^\beta + t_5 x_5 \rho^\gamma) J^2 \\
& + \frac{1}{16} (t_4 \rho^\beta - t_5 \rho^\gamma) \sum_{q=n,p} J_q^2. \quad (9)
\end{aligned}$$

Here, $\rho = \rho_n + \rho_p$, $\tau = \tau_n + \tau_p$, and $J = J_p + J_n$ are the particle number density, kinetic-energy density, and spin density, with p and n denoting the protons and neutrons, respectively. The Coulomb energy density can be expressed as

$$\mathcal{H}_{\text{Coul}} = \mathcal{H}_{\text{Coul}}^{\text{dir}} + \mathcal{H}_{\text{Coul}}^{\text{exc}}, \quad (10)$$

where $\mathcal{H}_{\text{Coul}}^{\text{dir}}$ is the direct term of the form

$$\mathcal{H}_{\text{Coul}}^{\text{dir}} = \frac{1}{2} e^2 \rho_p(r) \int \frac{\rho_p(r') d^3 r'}{|\mathbf{r} - \mathbf{r}'|}, \quad (11)$$

and $\mathcal{H}_{\text{Coul}}^{\text{exc}}$ is the exchange term

$$\mathcal{H}_{\text{Coul}}^{\text{exc}}(r) = -\frac{3}{4} e^2 \rho_p(r) \left(\frac{3\rho_p(r)}{\pi} \right)^{1/3}. \quad (12)$$

In the present work, we include the center-of-mass correction in the first order to the binding energy by modifying nucleon mass m to $mA/(A-1)$ with A the nucleon number. The pairing energy is evaluated in the constant gap approximation with the gap [59]

$$\Delta = \frac{11.2}{\sqrt{A}} \text{MeV}. \quad (13)$$

We would also like to point out that the contribution of spin current tensor term J^2 and J_q^2 are also included in our calculations.

B. Skyrme parameters and macroscopic quantities of nuclear matter

The expression Eq. (3) can be rewritten as

$$\begin{aligned}
\mathcal{H} = & \mathcal{K} + \mathcal{H}_0 + \mathcal{H}_3 + \mathcal{H}_{\text{eff}} + \frac{G_S}{2} (\nabla \rho)^2 - \frac{G_V}{2} (\nabla \rho_1)^2 \\
& - \frac{G_{SV}}{2} \delta \nabla \rho \nabla \rho_1 + \mathcal{H}_{\text{Coul}} + \mathcal{H}_{\text{SO}} + \mathcal{H}_{\text{sg}}, \quad (14)
\end{aligned}$$

where G_S is the gradient coefficient, G_V is the symmetry-gradient coefficient, G_{SV} is the cross gradient coefficient, and $\delta = \rho_1/\rho$ is the isospin asymmetry with $\rho_1 = \rho_n - \rho_p$. In the limit of infinite static nuclear matter, the sum of $\mathcal{K} + \mathcal{H}_0 + \mathcal{H}_3 + \mathcal{H}_{\text{eff}}$ corresponds to the energy density $\rho E(\rho, \delta)$ where $E(\rho, \delta)$ is just the EOS of asymmetric nuclear matter. Conventionally, some macroscopic quantities are introduced to characterize the EOS of asymmetric nuclear matter. For example, the $E(\rho, \delta)$ can be expanded as

$$E(\rho, \delta) = E_0(\rho) + E_{\text{sym}}(\rho)\delta^2 + \mathcal{O}(\delta^4), \quad (15)$$

where $E_0(\rho)$ is the EOS of symmetric nuclear matter and $E_{\text{sym}}(\rho)$ is the symmetry energy. The $E_0(\rho)$ is usually expanded around saturation density ρ_0 in terms of the incompressibility coefficient K_0 and the skewness coefficient J_0 as

$$E_0 = E_0(\rho_0) + \frac{1}{2!}K_0\chi^2 + \frac{1}{3!}J_0\chi^3 + \mathcal{O}(\chi^4), \quad (16)$$

with $\chi = (\rho - \rho_0)/3\rho_0$. Similarly, the $E_{\text{sym}}(\rho)$ can be expanded around a reference density ρ_r in terms of the density slope parameter L and the density curvature parameter K_{sym} as

$$\begin{aligned} E_{\text{sym}}(\rho) &= E_{\text{sym}}(\rho_r) + L(\rho_r)\chi_r \\ &+ \frac{1}{2!}K_{\text{sym}}(\rho_r)\chi_r^2 + \mathcal{O}(\chi_r^3), \end{aligned} \quad (17)$$

with $\chi_r = (\rho - \rho_r)/(3\rho_r)$. The $E_0(\rho_0)$, K_0 , J_0 , $E_{\text{sym}}(\rho_r)$, $L(\rho_r)$ and $K_{\text{sym}}(\rho_r)$ are six important macroscopic quantities that characterize the EOS of asymmetric nuclear matter.

Following the analysis method in the modified Skyrme-like (MSL) model with the standard Skyrme interaction [60, 61], the nine Skyrme parameters $t_0 \sim t_3$, $x_0 \sim x_3$ and α are expressed explicitly in terms of nine macroscopic quantities ρ_0 , $E_0(\rho_0)$, K_0 , $E_{\text{sym}}(\rho_r)$, $L(\rho_r)$, G_S , G_V , the isoscalar effective mass $m_{s,0}^*$ and isovector effective mass $m_{v,0}^*$. For the extended Skyrme interaction with thirteen Skyrme parameters in the present work, four additional macroscopic quantities are needed, and we use the skewness coefficient J_0 , the density curvature parameter of the symmetry energy $K_{\text{sym}}(\rho_r)$, the cross gradient coefficient G_{SV} and the Landau parameter $G'_0(\rho_0)$ of symmetric nuclear matter in the spin-isospin channel. Here J_0 and $K_{\text{sym}}(\rho_r)$, two higher-order quantities in nuclear matter EOS, may have important impacts on neutron star properties but are still poorly known [60, 62]. The coefficient G_{SV} vanishes in the standard SHF model. The Landau parameter G'_0 determines to the leading order the spin-isospin properties of nuclear matter and its value at saturation density can vary from about 0 to 1.6 depending on the models and methods [50, 63–69]. We present the explicit expressions of several macroscopic quantities in the SHF model with the extended Skyrme interactions in Appendix A.

And the analytical relations between the thirteen macroscopic quantities, i.e., ρ_0 , $E_0(\rho_0)$, K_0 , J_0 , $E_{\text{sym}}(\rho_r)$, $L(\rho_r)$, $K_{\text{sym}}(\rho_r)$, G_S , G_V , G_{SV} , $m_{s,0}^*$, $m_{v,0}^*$ and G'_0 , and the thirteen Skyrme parameters $t_0 \sim t_5$, $x_0 \sim x_5$ and α with β and γ fixed can be found in Appendix B.

The MSL method in which all the Skyrme parameters are expressed in terms of macroscopic quantities provides a simple approach to consider theoretical, experimental or empirical constraints on the selected macroscopic quantities for the properties of asymmetric nuclear matter. Another important advantage of the MSL method is that one can easily examine the correlation of experimental data or observations with each individual macroscopic quantities by varying individually these macroscopic quantities within their empirical ranges [61]. In the present work, instead of making correlation analysis, we shall focus on building parameter sets of the extended Skyrme interactions.

C. Landau parameters

The stability of nuclear matter can be investigated using the Landau Fermi-liquid theory. In this approach, for symmetric nuclear matter, the interaction $V(\mathbf{k}, \mathbf{k}')$ between two quasiparticles with momentum \mathbf{k} and \mathbf{k}' is a second-order variation of the energy density \mathcal{E} with respect to a variation of distribution function of the quasiparticles, which can be written as

$$\begin{aligned} V(\mathbf{k}, \mathbf{k}') &= \delta(\mathbf{r})N_0^{-1} \sum_l [F_l + F'_l \boldsymbol{\tau}_i \cdot \boldsymbol{\tau}_j + G_l \boldsymbol{\sigma}_i \cdot \boldsymbol{\sigma}_j \\ &+ G'_l (\boldsymbol{\tau}_i \cdot \boldsymbol{\tau}_j) (\boldsymbol{\sigma}_i \cdot \boldsymbol{\sigma}_j)] P_l(\cos\theta), \end{aligned} \quad (18)$$

where P_l is the Legendre polynomial, θ is the angle between \mathbf{k} and \mathbf{k}' , and N_0 is the level density at the Fermi surface defined as

$$N_0 = \frac{2m_s^* k_F}{\hbar^2 \pi^2}, \quad (19)$$

where $k_F = (3\pi^2\rho/2)^{1/3}$ is the Fermi momentum and m_s^* is the isoscalar effective mass at density ρ . F_l , F'_l , G_l and G'_l are the so-called dimensionless Landau parameters. For the Skyrme interaction containing only S and P wave contributions that we are considering in the present work, all Landau parameters vanish when $l > 1$. Therefore, there are eight Landau parameters for symmetric nuclear matter, i.e., F_l , F'_l , G_l and G'_l ($l = 0, 1$). Explicit expressions of the Landau parameters for the extended Skyrme energy functional can be found in Ref. [48].

The Landau stability conditions

$$F_l > -(2l + 1), \quad (20)$$

$$F'_l > -(2l + 1), \quad (21)$$

$$G_l > -(2l + 1), \quad (22)$$

$$G'_l > -(2l + 1), \quad (23)$$

guarantee the stability of symmetric nuclear matter against distortions of the momentum distribution functions in different channels. It is of particular interest to see that the conditions on F_0 , F'_0 , G_0 and G'_0 of symmetric nuclear matter ensure the stabilities of symmetric nuclear matter against spinodal instability, isospin instability, ferromagnetic instability and spin-isospin instability, respectively, which can be easily seen through the following relationships [50, 51]

$$\frac{\hbar^2 k_F^2}{3m_s^*}(1 + F_0) = \frac{\partial^2 \mathcal{E}(\rho, \rho_1, s_0, s_1)}{\partial \rho^2}, \quad (24)$$

$$\frac{\hbar^2 k_F^2}{3m_s^*}(1 + F'_0) = \frac{\partial^2 \mathcal{E}(\rho, \rho_1, s_0, s_1)}{\partial (\rho_1)^2} \bigg|_{\rho_1=s_0=s_1=0}, \quad (25)$$

$$\frac{\hbar^2 k_F^2}{3m_s^*}(1 + G_0) = \frac{\partial^2 \mathcal{E}(\rho, \rho_1, s_0, s_1)}{\partial (s_0)^2} \bigg|_{\rho_1=s_0=s_1=0}, \quad (26)$$

$$\frac{\hbar^2 k_F^2}{3m_s^*}(1 + G'_0) = \frac{\partial^2 \mathcal{E}(\rho, \rho_1, s_0, s_1)}{\partial (s_1)^2} \bigg|_{\rho_1=s_0=s_1=0}, \quad (27)$$

where \mathcal{E} represents the energy density of nuclear matter. Here, in the notation of Ref. [50], $\rho_1 = (\rho_n - \rho_p)$ is the isovector scalar density, $s_0 = (\rho_{n\uparrow} - \rho_{n\downarrow} + \rho_{p\uparrow} - \rho_{p\downarrow})$ is the isoscalar vector density and $s_1 = (\rho_{n\uparrow} - \rho_{n\downarrow} - \rho_{p\uparrow} + \rho_{p\downarrow})$ the isovector vector density with \uparrow (\downarrow) denoting spin-up (-down). For usual nuclear matter, one has the EOS $E(\rho, \delta) = \mathcal{E}(\rho, \rho_1, 0, 0)/\rho$, the incompressibility $K(\rho) = 18\rho \frac{\partial E}{\partial \rho} + 9\rho^2 \frac{\partial^2 E}{\partial \rho^2}$ and $E_{\text{sym}}(\rho) = \frac{1}{2} \frac{\partial^2 E}{\partial \delta^2} \big|_{\delta=0}$, and then one can obtain from Eqs. (24) and (25)

$$K(\rho) = \frac{3\hbar^2 k_F^2}{m_s^*}(1 + F_0), \quad (28)$$

$$E_{\text{sym}}(\rho) = \frac{\hbar^2 k_F^2}{6m_s^*}(1 + F'_0). \quad (29)$$

In addition, F_1 and F'_1 are directly related to the isoscalar and isovector effective masses through the following expressions [51]

$$\frac{m_s^*}{m} = 1 + \frac{F_1}{3}, \quad (30)$$

$$\frac{m_s^*}{m_v^*} = 1 + \frac{F'_1}{3}. \quad (31)$$

The conditions $F_1 > -3$ and $F'_1 > -3$ are thus naturally satisfied at arbitrary densities for positive isoscalar and isovector effective masses. Moreover, under the assumption $E \ll mc^2$, the sound velocity v_s in nuclear matter can be obtained from the relation $mv_s^2 \approx K(\rho)/9$, and thus in symmetric nuclear matter, from Eqs. (28) and (30), one can also express the v_s in terms of Landau parameters as [41]

$$mv_s^2 \approx \frac{\hbar^2 k_F^2}{3m} \frac{1 + F_0}{1 + \frac{1}{3}F_1}. \quad (32)$$

For pure neutron matter, there are only four Landau parameters $F_l^{(n)}$ and $G_l^{(n)}$ ($l = 0, 1$). Similarly the conditions $G_0^{(n)} > -1$ and $G_1^{(n)} > -3$ guarantee the stability

of pure neutron matter against spin polarization — or ferromagnetic transition. Explicit expressions for Landau parameters of pure neutron matter can be found in Ref. [51]. Generally, a critical density ρ_{cr} can be defined as the maximum density below which all the twelve Landau parameters of symmetric nuclear matter and pure neutron matter satisfy the stability conditions.

D. Isoscalar giant monopole resonance

The energy of the isoscalar giant monopole resonance (ISGMR) — or the breathing mode — perhaps is the most important and efficient probe of the incompressibility of nuclear matter around ρ_0 . Thus we also include in our following fit the experimental data of the ISGMR energy for several spherical nuclei. The ISGMR energy is evaluated as

$$E_{\text{GMR}} = \sqrt{\frac{m_1}{m_{-1}}}, \quad (33)$$

where m_i are i -th energy weighted sum rules defined as

$$m_i = \sum_{\nu} |\langle \nu | \hat{F} | 0 \rangle|^2 (E_{\nu})^i. \quad (34)$$

Here $|\nu\rangle$ is the RPA excitation state for the monopole operator $\hat{F} = \sum_i^A r_i^2$.

It is well established that the energy weighted sum rule m_1 can be evaluated as [70]

$$m_1 = 2 \frac{\hbar^2}{m} A \langle r^2 \rangle, \quad (35)$$

where A is the nucleon number, m is the nucleon mass and $\langle r^2 \rangle$ is the ground-state rms radius. The moment m_{-1} can be calculated through the constrained-HF (CHF) approach [71, 72]

$$m_{-1} = - \frac{1}{2} \frac{d}{d\lambda} \langle \lambda | r^2 | \lambda \rangle^2 \bigg|_{\lambda=0}, \quad (36)$$

where $|\lambda\rangle$ is the HF ground state for the CHF Hamiltonian $\hat{H} + \lambda \hat{F}$. In this work, we calculate the ISGMR energy using Eqs. (33), (35) and (36).

III. FITTING STRATEGY

In the present work, we use the simulated annealing method [63] to determine the parameters of the extended Skyrme interactions by minimizing the weighted sum of squared errors

$$\chi^2 = \sum_{i=1}^{N_d} \left(\frac{M_i^{\text{exp}} - M_i^{\text{th}}}{\sigma_i} \right)^2, \quad (37)$$

where N_d is the number of experimental data points, M_i^{exp} and M_i^{th} are the experimental and theoretical values for a selected observable, respectively, and σ_i is

the adopted error which is used to balance the relative weights of the various types of observables.

We include the following experimental data of a number of spherical even-even nuclei in our fit: (i) the binding energies E_B of ^{16}O , $^{40,48}\text{Ca}$, $^{56,68}\text{Ni}$, ^{88}Sr , ^{90}Zr , $^{100,116,132}\text{Sn}$, ^{144}Sm , ^{208}Pb [73]; (ii) the charge rms radii r_c of ^{16}O , $^{40,48}\text{Ca}$, ^{56}Ni , ^{88}Sr , ^{90}Zr , $^{116,132}\text{Sn}$, ^{144}Sm , ^{208}Pb [74, 75]; (iii) the ISGMR energies E_{GMR} of ^{90}Zr , ^{116}Sn , ^{144}Sm and ^{208}Pb [23]. To regulate the respective χ^2 for each sort of observable to be roughly equal to the number of corresponding data points, we assign a theoretical error 1.5 MeV to E_B , 0.015 fm to r_c while use the experimental error multiplied by a factor 3.54 for ISGMR energy E_{GMR} . In addition, the following constraints are considered in the optimization: (i) the critical density ρ_{cr} should be greater than 1.2 fm^{-3} ; (ii) the neutron $3p_{1/2} - 3p_{3/2}$ energy level splitting in ^{208}Pb should lie in the range of 0.8–1.0 MeV; (iii) the pressure of symmetric nuclear matter should be consistent with the constraints in the density region of $2\rho_0 < \rho < 4.6\rho_0$ obtained from analyzing flow data in heavy-ion collisions [26]; (iv) the EOS of pure neutron matter should conform to the predictions of the latest chiral effective field theory calculations with controlled uncertainties [14]. Furthermore, we fix the values of the magnitude $E_{\text{sym}}(\rho_c)$ and density slope $L(\rho_c)$ of the symmetry energy at $\rho_c = 0.11 \text{ fm}^{-3}$ to be equal to those extracted from the isotope binding energy difference [37] and the electric dipole polarizability in ^{208}Pb [76], i.e. $E_{\text{sym}}(\rho_c) = 26.65 \text{ MeV}$ and $L(\rho_c) = 47.3 \text{ MeV}$. For isoscalar and isovector effective masses at saturation density, $m_{s,0}^*$ and $m_{v,0}^*$, we consider three different cases: (i) $m_{s,0}^* = 0.9m$ and $m_{v,0}^* = 0.75m$ in parameter set eMSL09, which conform to the constraints we extracted recently from analyzing the giant resonances in ^{208}Pb [77]; (ii) $m_{s,0}^* = 0.8m$ and $m_{v,0}^* = 0.7m$ in parameter set eMSL08; (iii) $m_{s,0}^* = 0.7m$ and $m_{v,0}^* = 0.6m$ in parameter set eMSL07. For eMSL08 and eMSL07, the condition $m_{s,0}^* - m_{v,0}^* = 0.1m$ is imposed to be consistent with the extraction from global nucleon optical potentials constrained by world data on nucleon-nucleus and (p,n) charge-exchange reactions [78, 79].

IV. RESULTS AND DISCUSSIONS

Using the fitting procedure described in the previous section, we obtain three extended Skyrme interactions, namely, eMSL07, eMSL08 and eMSL09. Tab. I lists the values of the Skyrme parameters and the corresponding χ^2 . In the following, we discuss their performances in describing properties of finite nuclei, nuclear matter and neutron stars.

A. Properties of finite nuclei

In Fig. 1, we present the relative deviations of the binding energies and charge rms radii calculated with the

TABLE I: Skyrme parameters and χ^2 of the extended Skyrme parameter sets eMSL07, eMSL08 and eMSL09: lines 1–4 show the χ^2 evaluated from experimental data of binding energies, charge radii and ISGMR energies, namely $\chi_{E_B}^2$, $\chi_{r_c}^2$ and $\chi_{E_{\text{GMR}}}^2$, together with the total χ^2 , χ_{tot}^2 ; lines 5–18 show the Skyrme parameters. The last two lines show the calculated neutron skin thickness Δr_{np}^{208} and neutron $3p_{1/2} - 3p_{3/2}$ energy level splitting ϵ_{ls}^{208} of ^{208}Pb for the three interactions.

	eMSL07	eMSL08	eMSL09
χ_{tot}^2	25.13	24.39	23.40
$\chi_{E_B}^2$	12.89	10.38	8.16
$\chi_{r_c}^2$	8.24	9.55	10.73
$\chi_{E_{\text{GMR}}}^2$	4.01	4.46	4.50
$t_0 (\text{MeV} \cdot \text{fm}^3)$	-2708.55	-2307.26	-2211.66
$t_1 (\text{MeV} \cdot \text{fm}^5)$	574.272	488.825	431.684
$t_2 (\text{MeV} \cdot \text{fm}^5)$	-333.295	-421.424	-355.528
$t_3 (\text{MeV} \cdot \text{fm}^{3+3\alpha})$	15099.7	13872.9	14141.2
$t_4 (\text{MeV} \cdot \text{fm}^{5+3\beta})$	-747.989	-687.214	-692.363
$t_5 (\text{MeV} \cdot \text{fm}^{5+3\gamma})$	1028.48	822.790	612.570
x_0	0.363336	0.328931	0.279606
x_1	0.0614463	0.142688	0.219128
x_2	-0.623256	-0.680518	-0.474031
x_3	0.407087	0.329395	0.175182
x_4	0.0393223	0.0845719	0.113839
x_5	-0.692284	-0.593508	-0.296649
α	0.149523	0.208267	0.234192
β	1	1	1
γ	1	1	1
$W_0 (\text{MeV} \cdot \text{fm}^5)$	118.97	107.40	103.78
$\Delta r_{np}^{208} (\text{fm})$	0.182	0.182	0.183
$\epsilon_{ls}^{208} (\text{MeV})$	0.98	0.88	0.82

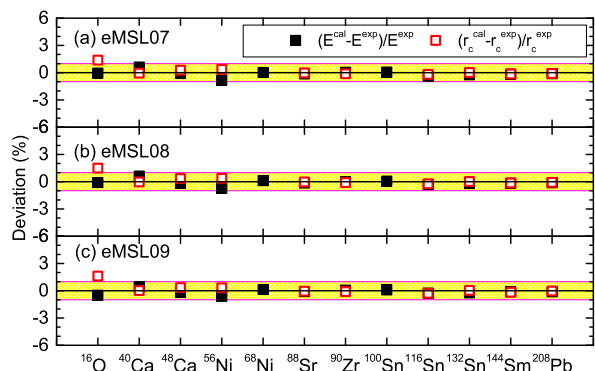


FIG. 1: (Color online) Deviations of the binding energies (solid squares) and charge rms radii (open squares) of a number of nuclei obtained from SHF with eMSL07, eMSL08 and eMSL09 from those measured in experiments [73–75]. The bands indicate a deviation within $\pm 1\%$.

three new interactions eMSL07, eMSL08 and eMSL09 from the corresponding experimental data [73–75]. The hatched bands indicate a deviation within $\pm 1\%$. One can see that all the three new interactions can describe the ground-state properties of finite nuclei very well (within $\pm 1\%$) except for the light nucleus ^{16}O for which the deviations of charge rms radius are slightly larger than 1% . Lines 1-3 in Tab. I also show that the variation of the effective masses has little impact on the fitting quality for the data of the binding energies and charge radii. Moreover, the χ^2 for the binding energy and charge radius calculated with the three interactions (see Table I) suggest that the binding energy data prefer a larger $m_{s,0}^*$ while the charge radius data favor a smaller $m_{v,0}^*$, and these features are consistent with the results in the SHF model with the standard Skyrme interactions [80].

The neutron skin thickness $\Delta r_{np} = \langle r_n^2 \rangle^{1/2} - \langle r_p^2 \rangle^{1/2}$, i.e., the difference of the neutron and proton rms radii, is of particular importance for the study of the density dependence of the symmetry energy. Mean field calculations using many different relativistic and nonrelativistic interactions have indicated that the neutron skin thickness is strongly correlated to the density slope $L(\rho_0)$ of the symmetry energy at saturations density [81–83]. Moreover, in Ref. [37], we find the neutron skin thickness of heavy nuclei is uniquely determined by $L(\rho_c)$ at a subsaturation density $\rho_c = 0.11 \text{ fm}^{-3}$. So we show in line 19 of Tab. I the neutron skin thickness of ^{208}Pb , Δr_{np}^{208} , predicted by HF calculations using the three new interactions. Due to the imposed condition $L(\rho_c) = 47.3 \text{ fm}$, the eMSL family predict quite similar values of Δr_{np}^{208} , i.e., about 0.18 fm , which are in very good agreement with the $\Delta r_{np}^{208} = 0.170 \pm 0.016 \text{ fm}$ and $\Delta r_{np}^{208} = 0.176 \pm 0.027 \text{ fm}$ from SHF analyses of neutron skin data of Sn isotopes [37] and experimental data of the electric dipole polarizability α_D in ^{208}Pb [76]. These results are also consistent with the estimated range $\Delta r_{np}^{208} = 0.165 \pm (0.009)_{\text{expt}} \pm (0.013)_{\text{theor}} \pm (0.021)_{\text{est}} \text{ fm}$ extracted from the measured α_D in ^{208}Pb [84], the constraint $\Delta r_{np}^{208} = 0.15 \pm 0.03(\text{stat.})_{-0.03}^{+0.01}(\text{sys.}) \text{ fm}$ from coherent pion photoproduction cross sections [85], and the constraint $\Delta r_{np}^{208} = 0.33_{-0.18}^{+0.16} \text{ fm}$ extracted from PREX at JLab [86].

The single-particle spectra are also important observables and have profound impact on the properties of

super-heavy nuclei [87]. However, it is known that the HF approach can not well describe the single-particle energies due to the self-interaction error [15], and thus we have not included them in our present fit. Unlike the single-particle energies, their differences among particle states or hole states (e.g., the spin-orbit splitting without crossing the shell gap), are believed to be robust observables which can be safely compared with the results of HF calculations [15]. Here we list in last line of Tab. I the neutron $3p_{1/2} - 3p_{3/2}$ energy level splitting in ^{208}Pb , ϵ_{ls}^{208} , for the eMSL family. As one can see, the results, especially $\epsilon_{ls}^{208} = 0.88 \text{ MeV}$ for eMSL08, well agree with the experimental value 0.89 MeV [17].

For the ISGMR energy, we show in Tab. II the calculated results together with the corresponding experimental data reported by TAMU group [23] and RCNP group [24, 25]. It can be seen that the three new interactions predict very similar and overall reasonable monopole response properties.

B. Properties of nuclear matter

In this subsection we discuss the properties of infinite nuclear matter predicted by the three new extended Skyrme interactions. We present in Tab. III the values of a number of macroscopic quantities in the SHF model with MSL07, eMSL08 and eMSL09. One can see that the three interactions predict very similar and reasonable macroscopic quantities at saturation density. In particular, the values of the magnitude and density slope of the symmetry, $E_{\text{sym}}(\rho_0)$ and $L(\rho_0)$, are essentially consistent with other constraints obtain from analyzing terrestrial experiments and astrophysical observations as well as the predictions of theoretical calculations [14, 88–91]. The calculated higher-order coefficients J_0 and $K_{\text{sym}}(\rho_0)$ are also in very good agreement with their empirical values [60, 62].

To see the nuclear matter properties more clearly, we show in Fig. 2 the pressure of symmetric nuclear matter $P_{\text{SNM}}(\rho)$, the binding energy per nucleus in pure neutron matter $E_{\text{PNM}}(\rho)$ and the symmetry energy $E_{\text{sym}}(\rho)$ as functions of densities for eMSL07, eMSL08 and eMSL09. For comparison, Fig. 2 also includes the constraints on $P_{\text{SNM}}(\rho)$ in the region of $2\rho_0$ - $4.6\rho_0$ from analyzing the flow data in relativistic heavy-ion collisions (Flow Data) [26]; the predictions on $E_{\text{PNM}}(\rho)$ at subsaturation densities from ChEFT calculations using next-to-next-to-next-to-leading order potential (ChEFT) [14]; the constraints on the density dependence of the symmetry energy at subsaturation densities from transport model analyses of mid-peripheral heavy-ion collisions of Sn isotopes (HIC) [40] and the SHF analyses of isobaric analog states (IAS) as well as combining additionally the neutron skin data (IAS+NSkin) [36]. In addition, the constraints (α_D in ^{208}Pb) on $E_{\text{PNM}}(\rho)$ and $E_{\text{sym}}(\rho)$ extracted recently from analyzing the electric dipole polarizability α_D in ^{208}Pb [39] are also displayed in Fig. 2 (b) and

TABLE II: Comparison of the ISGMR energies $E_{\text{GMR}} = \sqrt{m_1/m_{-1}}$ (in MeV) in ^{90}Zr , ^{116}Sn , ^{144}Sm and ^{208}Pb obtained for the eMSL07, eMSL08 and eMSL09 interactions with the experimental data [23–25].

Nucleus	TAMU	RCNP	eMSL07	eMSL08	eMSL09
^{90}Zr	17.81 ± 0.35	—	17.66	17.71	17.73
^{116}Sn	15.90 ± 0.07	15.70 ± 0.10	16.20	16.23	16.24
^{144}Sm	15.25 ± 0.11	—	15.29	15.29	15.31
^{208}Pb	14.18 ± 0.11	13.50 ± 0.10	13.57	13.54	13.55

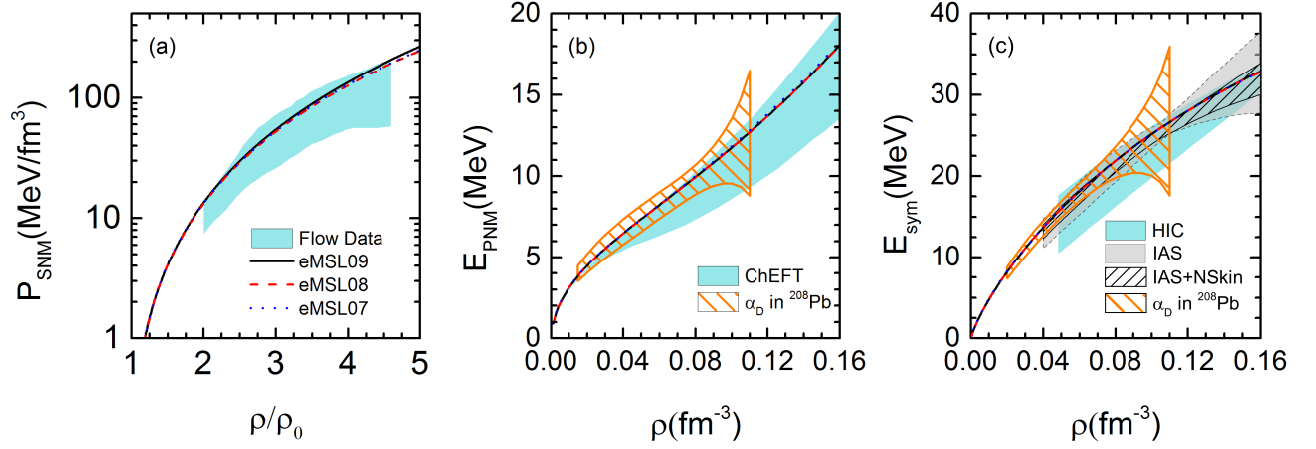


FIG. 2: (Color online) Pressure of symmetric nuclear matter $P_{\text{SNM}}(\rho)$ (a), the binding energy per nucleus of pure neutron matter $E_{\text{PNM}}(\rho)$ (b) and the symmetry energy $E_{\text{sym}}(\rho)$ (c) as functions of densities obtained from HF calculations using eMSL07, eMSL08 and eMSL09. Several constraints from analyzing experimental data and the predictions of theoretical calculations are also included for comparison (see text for details).

(c). It can be clearly seen that the HF calculations using the new family of extended Skyrme interactions are in very good agreement with all these constraints. We also notice that the eMSL family predict very similar symmetric nuclear matter properties even up to $5\rho_0$ as well as almost the same pure neutron matter EOS and the density dependence of the symmetry energy at subsaturation densities. As we mentioned before, the EOS of symmetric nuclear matter can be well constrained by the properties of finite nuclei and experimental data of heavy-ion collisions. It is not surprising to see that the three extended Skyrme interactions predict almost the

same $E_{\text{PNM}}(\rho)$ and $E_{\text{sym}}(\rho)$ at subsaturation densities, as the magnitude and density slope of the symmetry energy at $\rho_c = 0.11 \text{ fm}^{-3}$, namely $E_{\text{sym}}(\rho_c)$ and $L(\rho_c)$, are imposed to be 26.65 MeV and 47.3 MeV, respectively. This condition guarantees the eMSL family predict reasonable density dependence of the symmetry energy or the EOS of asymmetric nuclear matter at subsaturation densities and around ρ_0 .

For the high-density behaviors of the symmetry energy, we exhibit in the top panel of Fig. 3 the symmetry energy $E_{\text{sym}}(\rho)$ as a function of density up to 1 fm^{-3} for the eMSL family. One can see that the eMSL family predict a soft symmetry energy below and around saturation density but a stiff symmetry energy at supra-saturation densities. It is interesting to see that the symmetry energy predictions from the eMSL family are consistent with the constraint up to $3\rho_0$ obtained recently by extrapolating the well constrained subsaturation symmetry energy based on systematics of various relativistic and nonrelativistic EDFs [92]. Given the present poor knowledge on the high-density behaviors of the symmetry energy, we show in the bottom panel of Fig. 3 the comparison of the pure neutron matter EOS $E_{\text{PNM}}(\rho)$ as a function of density ρ from the eMSL family with the predictions of nonrelativistic BHF calculations using realistic Argonne V_{18} (A18) force [93] and the well known Akmal-Pandharipande-Ravenhall (APR) EOS using the realistic A18+ δv + UIX* interaction [9]. One can see that the three extended Skyrme interactions give very reasonable neutron matter EOSs that are consistent with the microscopic calculations. In particular, the EOS of pure neutron matter with eMSL09 is very close to the BHF EOS, while that with eMSL07 is very similar to the APR EOS.

We would like to emphasize that the main difference of nuclear matter properties for the three extended Skyrme interactions is the high-density behaviors of the EOS of

TABLE III: Macroscopic quantities in the SHF model with eMSL07, eMSL08 and eMSL09.

	eMSL07	eMSL08	eMSL09
$\rho_0(\text{fm}^{-3})$	0.1588	0.1588	0.1585
$E_0(\rho_0)(\text{MeV})$	-16.056	-16.048	-16.046
$K_0(\text{MeV})$	228.9	228.5	230.1
$J_0(\text{MeV})$	-360.0	-369.0	-353.7
$E_{\text{sym}}(\rho_c)(\text{MeV})$	26.65	26.65	26.65
$L(\rho_c)(\text{MeV})$	47.3	47.3	47.3
$K_{\text{sym}}(\rho_c)(\text{MeV})$	-96.4	-95.2	-92.1
$G_S(\text{MeV}\cdot\text{fm}^5)$	120.6	105.6	92.9
$G_V(\text{MeV}\cdot\text{fm}^5)$	49.0	50.9	46.2
$G_{SV}(\text{MeV}\cdot\text{fm}^5)$	-8.0	-8.0	-8.4
$G'_0(\rho_0)$	0.28	0.18	0.25
$m_{s,0}^*/m$	0.7	0.8	0.9
$m_{v,0}^*/m$	0.6	0.7	0.75
$E_{\text{sym}}(\rho_0)(\text{MeV})$	32.7	32.8	32.8
$L(\rho_0)(\text{MeV})$	51.7	52.4	53.7
$K_{\text{sym}}(\rho_0)(\text{MeV})$	-130.0	-119.8	-100.2

asymmetric nuclear matter or the symmetry energy. This is partly because the variation of $m_{s,0}^*$ and $m_{v,0}^*$ values in different extended Skyrme interactions, which has essential impacts on the \mathcal{H}_{eff} (i.e., Eq. (6)) and is related to the momentum dependence of the three body forces. Therefore, the additional momentum and density dependent two-body forces which effectively simulate the momentum dependence of the three-body force may play an important role for the high-density behaviors of the EOS of asymmetric nuclear matter.

C. Landau parameters

We calculate the density dependence of the Landau parameters of symmetric nuclear matter and pure neutron matter according to the explicit expressions in Refs. [48, 51] and the results are exhibited in Fig. 4 and Fig. 5, respectively. One can see that for the three extended Skyrme interactions, all the Landau parameters, except F_0 for symmetric nuclear matter, satisfy the stability conditions at densities up to 1.2 fm^{-3} and thus guarantee the stability of symmetric nuclear matter and pure neutron matter from subsaturation densities to very high densities. The instability of symmetric nuclear matter at densities below about 0.1 fm^{-3} determined by the

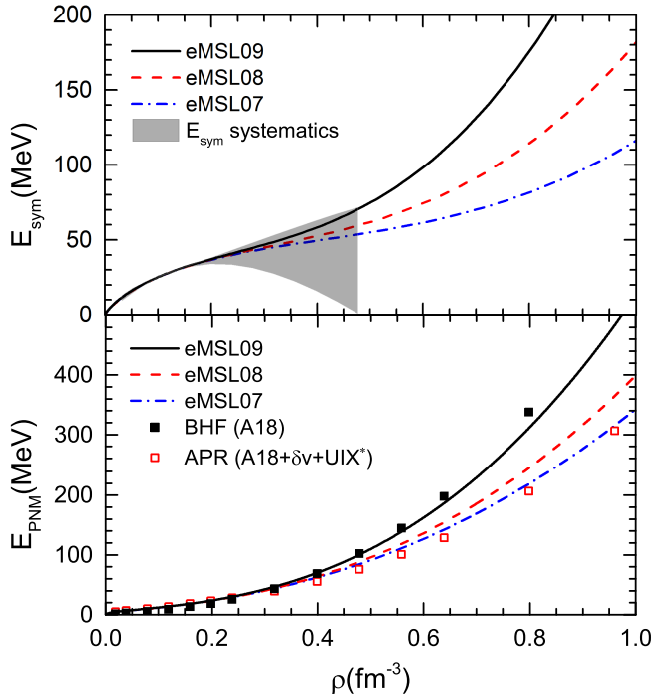


FIG. 3: (Color online) Density dependence of the symmetry energy $E_{\text{sym}}(\rho)$ (top panel) and EOSs of pure neutron matter $E_{\text{PNM}}(\rho)$ (bottom panel) with the extended Skyrme interactions eMSL07, eMSL08 and eMSL09. The shaded band in the top panel is taken from Ref. [92]. The $E_{\text{PNM}}(\rho)$ of APR is taken from Ref. [9] while that of BHF is from Ref. [93].

TABLE IV: Landau parameters of symmetric nuclear matter and pure neutron matter at saturation density in the SHF model with eMSL07, eMSL08 and eMSL09.

	eMSL07	eMSL08	eMSL09
F_0	-0.27	-0.17	-0.057
F'_0	0.88	1.14	1.42
F_1	-0.90	-0.60	-0.30
F'_1	0.50	0.43	0.60
G_0	0.061	0.18	-0.21
G'_0	0.28	0.18	0.25
G_1	0.38	0.15	0.18
G'_1	0.63	0.77	0.75
$F_0^{(n)}$	0.064	0.19	0.52
$F_1^{(n)}$	-0.48	-0.20	0.37
$G_0^{(n)}$	-0.19	-0.14	-0.40
$G_1^{(n)}$	1.21	1.07	1.16

value of F_0 corresponds to the well-known spinodal instability, which is physical and is believed to be related to the liquid-gas phase transition in nuclear matter and the multifragmentation phenomenon observed in heavy-ion collisions at intermediate energies [94, 95]. In the spinodal unstable region of symmetric nuclear matter, the squared sound velocity or the incompressibility of symmetric nuclear matter is negative (see, e.g., Eq. (32) and the relation $mv_s^2 \approx K(\rho)/9$). At densities beyond 1.2 fm^{-3} , both symmetric nuclear matter and pure neutron matter become unstable in the spin-isospin channels,

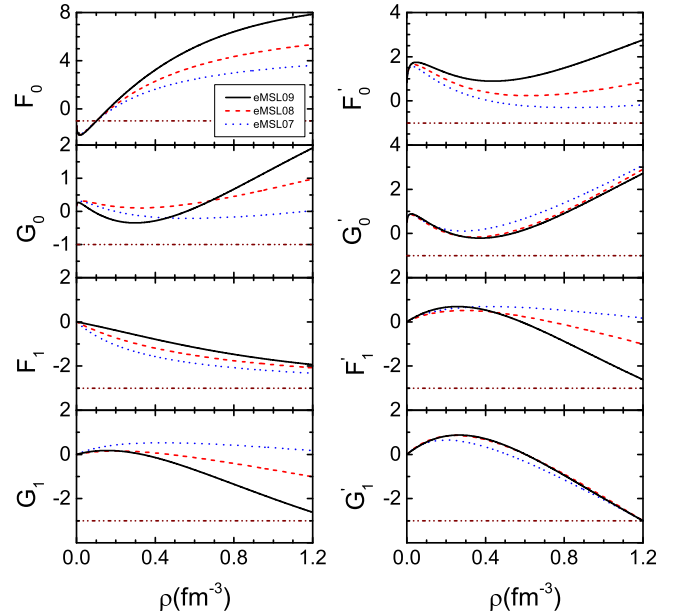


FIG. 4: (Color online) Density dependence of the Landau parameters of symmetric nuclear matter for the extended Skyrme interactions eMSL07, eMSL08 and eMSL09. The dash-dotted lines indicate stability conditions.

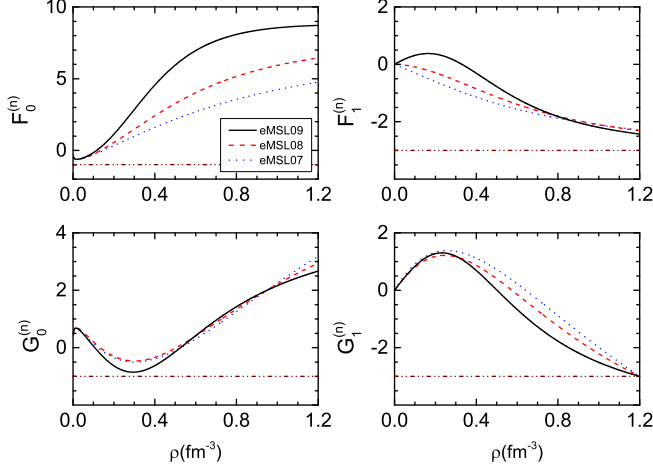


FIG. 5: (Color online) Similar to Fig. 4 but for pure neutron matter.

and the density $\rho = 1.2 \text{ fm}^{-3}$ is thus the critical density. This large value of the critical density ensure the extended Skyrme interactions obtained in the present work can be used safely to calculate the structure of neutron stars. As we will see later, the center densities of the neutron stars with largest mass configuration obtained with eMSL07, eMSL08 and eMSL09 are all less than $\rho = 1.2 \text{ fm}^{-3}$.

To close this subsection, we list in Tab. IV the values of all the twelve Landau parameters of nuclear matter at saturation density in the SHF model with the eMSL family.

D. Neutron star properties

In the following, we discuss the mass-radius relation of static neutron stars, which is obtained by solving the famous Tolman-Oppenheimer-Volkov (TOV) equation [96, 97], i.e.,

$$\frac{dP(r)}{dr} = -\frac{G}{c^2 r^2} \left[\epsilon(r) + \frac{P(r)}{c^2} \right] \times \left[M(r) + 4\pi r^3 \frac{P(r)}{c^2} \right] \left[1 - \frac{2GM(r)}{c^2 r} \right]^{-1} \quad (38)$$

$$\frac{dM(r)}{dr} = 4\pi \epsilon(r) r^2 / c^2, \quad (39)$$

where r is the radial coordinate, $M(r)$ is the gravitational mass inside the sphere of radius r , $\epsilon(r)$ and $P(r)$ are, respectively, the corresponding energy density and pressure of the neutron star matter at r , and G is Newton's gravitational constant,

To solve the TOV equation, an EOS of neutron star matter $P(\epsilon)$ is necessary. In the present work, we assume the core of neutron stars consists of neutron, proton, electrons and possible muons without phase transition and other degrees of freedom at high densities. Then the EOS

TABLE V: Maximum mass of the neutron star (M_{max}), the center density of the maximum mass neutron star configuration ($\rho_{\text{max}}^{\text{cen}}$), the radius of $1.4M_{\odot}$ neutron star ($R_{1.4}$), and core-crust transition density of the neutron star (ρ_t) for eMSL07, eMSL08 and eMSL09.

	eMSL07	eMSL08	eMSL09
M_{max}/M_{\odot}	2.12	2.15	2.21
$\rho_{\text{max}}^{\text{cen}} (\text{fm}^{-3})$	1.15	1.10	1.03
$R_{1.4} (\text{km})$	12.2	12.3	12.6
$\rho_t (\text{fm}^{-3})$	0.077	0.078	0.079

of neutron star matter is constructed in the following way: for the core, we calculate the EOS of $npe\mu$ matter in SHF model using the extended Skyrme interactions; for the outer crust, we use the EOS of BPS (FMT) in the region of $6.93 \times 10^{-13} \text{ fm}^{-3} < \rho < \rho_{\text{out}}$ ($4.73 \times 10^{-15} \text{ fm}^{-3} < \rho < 6.93 \times 10^{-13} \text{ fm}^{-3}$) [98]; for the inner crust in the region between ρ_{out} and ρ_t we construct its EOS by interpolating with the form [99, 100]

$$P = a + b\epsilon^{4/3}. \quad (40)$$

Here $\rho_{\text{out}} = 2.46 \times 10^{-14} \text{ fm}^{-3}$ is the critical density between the inner and the outer crust, and ρ_t is the core-crust transition density which is evaluated self-consistently using the extended Skyrme interactions within the thermodynamic method (see, e.g., Ref. [100]).

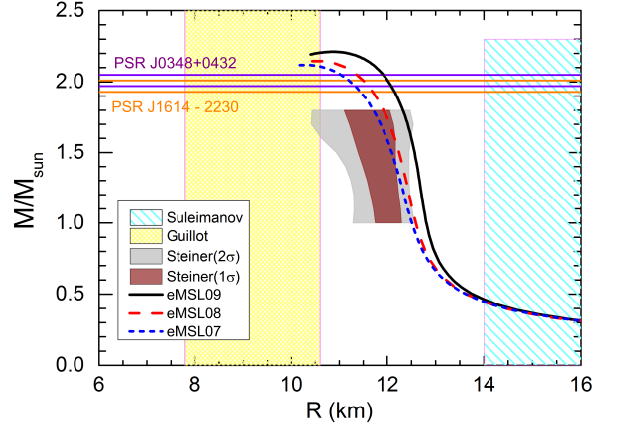


FIG. 6: (Color online) Mass-radius relation of neutron stars predicted from eMSL07, eMSL08 and eMSL09. Some recent observational constraints [21, 22, 101–103] are also included for comparison.

We present in Tab. V the maximum mass M_{max} , the center density $\rho_{\text{max}}^{\text{cen}}$ of the maximum mass neutron star configuration, the radius of $1.4M_{\odot}$ neutron star $R_{1.4}$ and the core-crust transition density ρ_t . It can be seen that all three extended Skyrme interactions can successfully support $2M_{\odot}$ neutron stars and the interaction with a stiffer symmetry energy at high-density region predicts a larger maximum mass and a larger stellar radius for a

canonical neutron star with mass of $1.4M_{\odot}$. In addition, as mentioned earlier, the values of $\rho_{\text{max}}^{\text{cen}}$ for the three extended Skyrme interactions are all less than the critical density of $\rho_{\text{crit}} = 1.2 \text{ fm}^{-3}$. For the core-crust transition density ρ_t , which is essentially determined by $L(\rho_c)$ or $L(\rho_0)$ [61, 76], the three extended Skyrme interactions also produce very similar values that are consistent with the empirical value [1].

Shown in Fig. 6 is the mass-radius relation of neutron stars predicted from eMSL09, eMSL08 and eMSL07. The horizontal bands in Fig. 6 indicate the measured masses $M = 1.97 \pm 0.04M_{\odot}$ [21] and $M = 2.01 \pm 0.04M_{\odot}$ [22] of the two heaviest neutron stars PSR J1614-2230 [21] and PSR J0348+0432 [22], respectively. For comparison, we also show in Fig. 6 the constraints on the radii of neutron stars by Steiner *et al.* from analyses of three X-ray bursters and three transient low-mass X-ray binaries [101]. However, by analyzing the same data sets using more sophisticated atmospheres models, Suleimanov *et al.* concluded that the lower limit on the stellar radius is 14 km for masses bellow $2.3M_{\odot}$ [102]. Indeed, large systematic uncertainties in the analysis of x-ray bursters have hindered the reliability of these results. A cleaner way to extract the radii of neutron stars is from the observation of quiescent low mass x-ray binaries (qLMXB) in globular clusters. By assuming the neutron star radius is independent on mass, namely $R(M) = R_0$, Guillet *et al.* [103] determined a rather small stellar radius of $R_0 = 9.1^{+1.3}_{-1.5} \text{ km}$ within 90% confidence level from fitting the spectra of five qLMXBs. Note that the assumption $R(M) = R_0$ is rather strong and prior conditions of causality and $2M_{\odot}$ neutron stars may change the result [104]. Therefore, the accurate determination of the radius of neutron stars, which can put a stringent constraint on the density dependence of the symmetry energy beyond saturation density [105], is still a big challenge. The predicted radii of the $1.4M_{\odot}$ neutron star ($\sim 12.5 \text{ km}$) from the eMSL family are in very good agreement with recent predictions from the studies based nuclear experiments and theoretical calculations of pure neutron matter (see, e.g., Ref. [104] and references therein).

V. CONCLUSIONS

Within the framework of the extended Skyrme interaction which includes additional momentum and density dependent terms to simulate the momentum dependence of the three-body force, we have constructed three new extended Skyrme interactions, namely, eMSL07, eMSL08 and eMSL09, by fitting of the data of finite nuclei and the properties of nuclear matter with the simulated annealing method. We have shown that the eMSL family of extended Skyrme interactions can well reproduce both the ground-state properties and ISGMR energies of finite nuclei, and conform to various most recent constraints on nuclear matter EOS from theory, experiment

and observation. The high-density EOSs of pure neutron matter for the three extended Skyrme interactions are also consistent with the predictions of the microscopic calculations using realistic nuclear forces. Moreover, the extended Skyrme interactions successfully eliminate the unphysical instabilities in nuclear matter at densities up to about $7.5\rho_0$. Therefore, the eMSL family constructed in the present work are very suitable for the study of neutron stars.

We have used the three new extended Skyrme interactions to study the mass-radius relation of neutron stars and our results indicate that the eMSL family can support $2M_{\odot}$ neutron stars and predict very reasonable stellar radii. Our present work shows that the momentum dependence of the three-body force may play an important role in improving the SHF description of nuclear matter, finite nuclei and neutron stars. The new family of the extended Skyrme interactions constructed in the present work provide a unified approach to understand the properties of asymmetric nuclear matter from sub- to supra-saturation densities in large isospin region and are thus appropriate for the study of nuclear matter, finite nuclei and neutron stars.

Acknowledgments

This work was supported in part by the Major State Basic Research Development Program (973 Program) in China under Contract Nos. 2013CB834405 and 2015CB856904, the NNSF of China under Grant Nos. 11275125 and 11135011, the “Shu Guang” project supported by Shanghai Municipal Education Commission and Shanghai Education Development Foundation, the Program for Professor of Special Appointment (Eastern Scholar) at Shanghai Institutions of Higher Learning, and the Science and Technology Commission of Shanghai Municipality (11DZ2260700).

Appendix A: Macroscopic quantities in the extended SHF model

In the SHF model with the extended Skyrme interaction given in Eqs. (1) and (2), the EOS of asymmetric

nuclear matter can be expressed as

$$\begin{aligned}
E(\rho, \delta) = & \frac{3\hbar^2}{10m} k_F^2 F_{5/3} \\
& + \frac{1}{8} t_0 \rho [2(x_0 + 2) - (2x_0 + 1)F_2] \\
& + \frac{1}{48} t_3 \rho^{\alpha+1} [2(x_3 + 2) - (2x_3 + 1)F_2] \\
& + \frac{3}{40} \rho k_F^2 \left\{ [t_1(x_1 + 2) + t_2(x_2 + 2)] F_{5/3} \right. \\
& + \left. \frac{1}{2} [t_2(2x_2 + 1) - t_1(2x_1 + 1)] F_{8/3} \right\} \\
& + \frac{3}{40} \rho k_F^2 \left\{ [t_4(x_4 + 2)\rho^\beta + t_5(x_5 + 2)\rho^\gamma] F_{5/3} \right. \\
& + \left. \frac{1}{2} [t_5(2x_5 + 1)\rho^\gamma - t_4(2x_4 + 1)\rho^\beta] F_{8/3} \right\} \quad (A1)
\end{aligned}$$

where m is the nucleon mass, k_F is the Fermi momentum of symmetric nuclear matter, i.e.,

$$k_F = \left(\frac{3\pi^2 \rho}{2} \right)^{1/3}, \quad (A2)$$

and $F_x(\delta)$ is expressed as

$$F_x(\delta) = \frac{1}{2} [(1 + \delta)^x + (1 - \delta)^x]. \quad (A3)$$

By setting $\delta = 0$ in Eq. (A1), one can obtain the EOS of symmetric nuclear matter as

$$\begin{aligned}
E_0(\rho) = & \frac{3\hbar^2}{10m} k_F^2 + \frac{3}{8} t_0 \rho + \frac{1}{16} t_3 \rho^{\alpha+1} \\
& + \frac{3}{80} [3t_1 + t_2(4x_2 + 5)] \rho k_F^2 \\
& + \frac{3}{80} [3t_4 \rho^\beta + t_5(4x_5 + 5)\rho^\gamma] \rho k_F^2. \quad (A4)
\end{aligned}$$

The incompressibility K_0 and skewness parameter J_0 of symmetric nuclear matter can then be easily derived with the following definitions

$$K_0 \equiv 9\rho_0^2 \left. \frac{d^2 E_0(\rho)}{d\rho^2} \right|_{\rho=\rho_0}, \quad (A5)$$

$$J_0 \equiv 27\rho_0^3 \left. \frac{d^3 E_0(\rho)}{d\rho^3} \right|_{\rho=\rho_0}. \quad (A6)$$

The symmetry energy is given by

$$\begin{aligned}
E_{\text{sym}}(\rho) \equiv & \frac{1}{2} \left. \frac{\partial^2 E(\rho, \delta)}{\partial \delta^2} \right|_{\delta=0} \\
= & \frac{\hbar^2}{6m} k_F^2 - \frac{1}{8} t_0 (2x_0 + 1) \rho \\
& - \frac{1}{48} t_3 (2x_3 + 1) \rho^{\alpha+1} \\
& - \frac{1}{24} [3t_1 x_1 - t_2 (4 + 5x_2)] \rho k_F^2 \\
& - \frac{1}{24} [3t_4 x_4 \rho^\beta - t_5 (4 + 5x_5) \rho^\gamma] \rho k_F^2, \quad (A7)
\end{aligned}$$

and the density slope of the symmetry energy at a reference density ρ_r can be obtained by the following definition

$$L(\rho_r) \equiv 3\rho_r \left. \frac{dE_{\text{sym}}(\rho)}{d\rho} \right|_{\rho=\rho_r}. \quad (A8)$$

In the extended SHF model, the isoscalar effective mass $m_{s,0}^*$, namely, the effective mass of nucleon in symmetric nuclear matter at saturation density is evaluated by the following relation

$$\begin{aligned}
\frac{\hbar^2}{2m_{s,0}^*} = & \frac{\hbar^2}{2m} + \frac{3}{16} t_1 \rho_0 + \frac{1}{16} t_2 (4x_2 + 5) \rho_0 \\
& + \frac{3}{16} t_4 \rho_0^{\beta+1} + \frac{1}{16} t_5 (4x_5 + 5) \rho_0^{\gamma+1}. \quad (A9)
\end{aligned}$$

The value of the isovector effective mass $m_{v,0}^*$, namely, the effective mass of neutron (proton) in pure proton (neutron) matter at saturation density is given by

$$\begin{aligned}
\frac{\hbar^2}{2m_{v,0}^*} = & \frac{\hbar^2}{2m} + \frac{1}{8} t_1 (x_1 + 2) \rho_0 + \frac{1}{8} t_2 (x_2 + 2) \rho_0 \\
& + \frac{1}{8} t_4 (x_4 + 2) \rho_0^{\beta+1} + \frac{1}{8} t_5 (x_5 + 2) \rho_0^{\gamma+1} \quad (A10)
\end{aligned}$$

For the finite-range term \mathcal{H}_{fin} in Eq. (3), the gradient coefficient G_S , the symmetry gradient coefficient G_V and the cross gradient coefficient G_{SV} can be obtained as

$$\begin{aligned}
G_S = & \frac{9}{32} t_1 - \frac{1}{32} t_2 (4x_2 + 5) \\
& + \frac{3}{32} t_4 (2\beta + 3) \rho^\beta - \frac{1}{32} t_5 (4x_5 + 5) \rho^\gamma, \quad (A11)
\end{aligned}$$

$$\begin{aligned}
G_V = & \frac{3}{32} t_1 (2x_1 + 1) + \frac{1}{32} t_2 (2x_2 + 1) \\
& + \frac{3}{32} t_4 (2x_4 + 1) \rho^\beta + \frac{1}{32} t_5 (2x_5 + 1) \rho^\gamma, \quad (A12)
\end{aligned}$$

$$G_{SV} = \frac{\beta}{16} t_4 (1 + 2x_4) \rho^\beta. \quad (A13)$$

Appendix B: Relationship between the Skyrme parameters and the macroscopic quantities in the extended SHF model

We reexpress the EOS of symmetric nuclear matter (Eq. (A4)) as

$$\begin{aligned}
E_0(\rho) = & E_{\text{kin}}^0 \left(\frac{\rho}{\rho_0} \right)^{2/3} + s_0 \frac{\rho}{\rho_0} + (s_1 + s_2) \left(\frac{\rho}{\rho_0} \right)^{5/3} \\
& + s_3 \left(\frac{\rho}{\rho_0} \right)^{\alpha+1} + s_4 \left(\frac{\rho}{\rho_0} \right)^{\beta+5/3} + s_5 \left(\frac{\rho}{\rho_0} \right)^{\gamma+5/3} \quad (B1)
\end{aligned}$$

where we have

$$E_{\text{kin}}^0 = \frac{3\hbar^2}{10m} k_{F,0}^2, \quad (B2)$$

with $k_{F,0} = (3\pi^2\rho_0/2)^{1/3}$ and the coefficients $s_0 \sim s_5$ are defined as

$$\begin{aligned} s_0 &= \frac{3}{8}t_0\rho_0, & s_3 &= \frac{1}{16}t_3\rho_0^{\alpha+1}, \\ s_1 &= \frac{9}{80}t_1\rho_0k_{F,0}^2, & s_4 &= \frac{9}{80}t_4\rho_0^{\beta+1}k_{F,0}^2, \\ s_2 &= \frac{3}{80}t_2(5+4x_2)\rho_0k_{F,0}^2, & s_5 &= \frac{3}{80}t_5(5+4x_5)\rho_0^{\gamma+1}k_{F,0}^2. \end{aligned}$$

Similarly, the symmetry energy (Eq. (A7)) can be rewritten as

$$\begin{aligned} E_{\text{sym}}(\rho) &= E_{\text{kin}}^{\text{sym}}\left(\frac{\rho}{\rho_0}\right)^{2/3} + \omega_0\frac{\rho}{\rho_0} + (\omega_1 + \omega_2)\left(\frac{\rho}{\rho_0}\right)^{5/3} \\ &+ \omega_3\left(\frac{\rho}{\rho_0}\right)^{\alpha+1} + \omega_4\left(\frac{\rho}{\rho_0}\right)^{\beta+5/3} + \omega_5\left(\frac{\rho}{\rho_0}\right)^{\gamma+5/3}, \end{aligned} \quad (\text{B3})$$

where we have

$$E_{\text{kin}}^{\text{sym}} = \frac{\hbar^2}{6m}k_{F,0}^2 \quad (\text{B4})$$

and the coefficients $\omega_0 \sim \omega_5$ are defined as

$$\begin{aligned} \omega_0 &= -\frac{1}{8}t_0(2x_0+1)\rho_0, & \omega_3 &= \frac{1}{48}t_3(2x_3+1)\rho_0^{\alpha+1}, \\ \omega_1 &= -\frac{1}{8}t_1x_1\rho_0k_{F,0}^2, & \omega_4 &= -\frac{1}{8}t_4x_4\rho_0^{\beta+1}k_{F,0}^2, \\ \omega_2 &= \frac{1}{24}t_2(4+5x_2)\rho_0k_{F,0}^2, & \omega_5 &= \frac{1}{24}t_5(4+5x_5)\rho_0^{\gamma+1}k_{F,0}^2. \end{aligned}$$

In the extended SHF model with fixed β and γ , the thirteen coefficients $s_0 \sim s_5$, $\omega_0 \sim \omega_5$ and α can be explicitly expressed in terms of thirteen macroscopic quantities ρ_0 , $E_0(\rho_0)$, K_0 , J_0 , $E_{\text{sym}}(\rho_r)$, $L(\rho_r)$, $K_{\text{sym}}(\rho_r)$, G_S , G_V , G_{SV} , G'_0 , $m_{s,0}^*$ and $m_{v,0}^*$. Before showing the explicit expressions, we define

$$\begin{aligned} \xi_1 &= E_{\text{kin}}^0 \frac{m - m_{s,0}^*}{m_{s,0}^*}, & \xi_2 &= \frac{20}{9}\xi_1 - \frac{\hbar^2}{2m} \frac{m - m_{v,0}^*}{m_{v,0}^*} k_{F,0}^2, \\ A'_0 &= \frac{27\hbar^2\pi^2 G'_0 \rho_0}{4m_{s,0}^* k_{F,0}^2}, & A_S &= \frac{6}{5}G_S \rho_0 k_{F,0}^2, \\ A_V &= 18G_V \rho_0 k_{F,0}^2, & A_{SV} &= \frac{1}{\beta}G_{SV} \rho_0 k_{F,0}^2. \end{aligned}$$

The $s_0 \sim s_5$, $\omega_0 \sim \omega_5$ and α can then be expressed as

$$\begin{aligned} s_4 &= \frac{1}{2\beta}(A_S + 4Y_1 - 3\xi_1), \\ s_1 &= \xi_1 - Y_1 - s_4, \\ \alpha &= \frac{-Y_b + \sqrt{Y_b^2 - 4Y_a \cdot Y_c}}{2Y_a}, \\ s_3 &= \frac{27Y_a}{\alpha(3\alpha - 3\gamma - 4)}, \\ s_5 &= [K_0 + 2E_{\text{kin}}^0 - 10\xi_1 - (3\alpha + 3)(E_{\text{kin}} - 3E_0 - 2\xi_1) \\ &\quad - 3\beta(3\beta - 3\alpha + 4)s_4] / [3\gamma(3\gamma - 3\alpha + 4)], \\ s_0 &= E_0 - E_{\text{kin}}^0 - \xi_1 - s_3, \\ s_2 &= Y_1 - s_5, \end{aligned}$$

$$\begin{aligned} \omega_4 &= \frac{5}{9}s_4 - A_{SV}, \\ \omega_1 &= -\omega_4 - \frac{A'_0}{54} - \frac{A_V}{27} - \frac{E_0}{6} + \frac{E_{\text{kin}}^0}{6} + \frac{4}{9}\xi_1, \\ \omega_3 &= \left\{ Y_2 \left[(3\gamma + 2)(3\gamma + 5)\eta^{\gamma+5/3} - 10\eta^{5/3} \right] \right. \\ &\quad \left. - Y_3 \left[(3\gamma + 2)\eta^{\gamma+5/3} - 2\eta^{5/3} \right] \right\} \\ &\quad / \left\{ 3\alpha\eta^{\alpha+1}[(3\gamma + 2)(3\gamma - 3\alpha + 2)\eta^{\gamma+5/3} \right. \\ &\quad \left. + (6\alpha - 4)\eta^{5/3}] \right\}, \\ \omega_5 &= [Y_3 - Y_2(3\alpha + 3)] \\ &\quad / \left[(3\gamma + 2)(3\gamma - 3\alpha + 2)\eta^{\gamma+5/3} + 2(3\alpha - 2)\eta^{5/3} \right], \\ \omega_2 &= -\frac{A'_0}{18} - \frac{E_0}{2} + \frac{E_{\text{kin}}^0}{2} - \frac{\xi_1}{3} + \frac{20}{9}Y_1 - \omega_5, \\ \omega_0 &= \eta^{-1}E_{\text{sym}}(\rho_r) - \eta^{-1/3}E_{\text{kin}}^{\text{sym}} - \eta^\alpha\omega_3 \\ &\quad - \eta^{2/3}(\omega_1 + \omega_2) - \eta^{\beta+2/3}\omega_4 - \eta^{\gamma+2/3}\omega_5, \end{aligned}$$

with

$$\begin{aligned} \eta &= \frac{\rho_r}{\rho_0}, \\ Y_1 &= \frac{1}{30}A'_0 + \frac{1}{60}A_V + \frac{3}{10}E_0 - \frac{3}{10}E_{\text{kin}}^0 - \frac{1}{20}\xi_1 + \frac{9}{20}\xi_2, \\ Y_2 &= L(\rho_r) - 3E_{\text{sym}}(\rho_r) + \eta^{2/3}E_{\text{kin}}^{\text{sym}} - 2\eta^{5/3}\xi_2 \\ &\quad + \omega_4[2\eta^{5/3} - (3\beta + 2)\eta^{\beta+5/3}], \\ Y_3 &= K_{\text{sym}}(\rho_r) + 2\eta^{2/3}E_{\text{kin}}^{\text{sym}} - 10\eta^{5/3}\xi_2 + \\ &\quad \omega_4[10\eta^{5/3} - (3\beta + 2)(3\beta + 5)\eta^{\beta+5/3}], \\ Y_a &= 9[K_0 + 2E_{\text{kin}}^0 - 10\xi_1 - (3\gamma + 7)(E_{\text{kin}}^0 - 3E_0 - 2\xi_1) \\ &\quad - 9\beta(\beta - \gamma)s_4], \\ Y_b &= 9(3\gamma^2 + 6\gamma + 1)(E_{\text{kin}}^0 - 3E_0 - 2\xi_1 - 3\beta s_4) \\ &\quad - 3[J_0 - 8E_{\text{kin}}^0 + 10\xi_1 - 9\beta(3\beta^2 + 6\beta + 1)s_4], \\ Y_c &= -Y_a - 3(3\gamma^2 + 6\gamma + 1) \\ &\quad \times [K_0 - E_{\text{kin}}^0 + 9E_0 - 4\xi_1 - 3\beta(3\beta + 4)s_4] \\ &\quad + (3\gamma + 4)[J_0 - 8E_{\text{kin}}^0 + 10\xi_1 - 9\beta(3\beta^2 + 6\beta + 1)s_4]. \end{aligned}$$

Once given the thirteen macroscopic quantities, one can obtain $s_0 \sim s_5$, $\omega_0 \sim \omega_5$ and α by invoking the above expressions, and then the Skyrme parameters can be easily obtained.

-
- [1] J.M. Lattimer and M. Prakash, *Science* **304**, 536 (2004); *Phys. Rep.* **442**, 109 (2007).
 - [2] A.W. Steiner, M. Prakash, J.M. Lattimer, and P. J. Ellis, *Phys. Rep.* **411**, 325 (2005).
 - [3] V. Baran, M. Colonna, V. Greco, and M. Di Toro, *Phys. Rep.* **410**, 335 (2005).
 - [4] B.A. Li, L.W. Chen, and C.M. Ko, *Phys. Rep.* **464**, 113 (2008).
 - [5] B. ter Haar and R. Malfliet, *Phys. Rep.* **149**, 207 (1987).
 - [6] I. Bombaci and U. Lombardo, *Phys. Rev. C* **44**, 1892 (1991).
 - [7] W. Zuo, I. Bombaci and U. Lombardo, *Phys. Rev. C* **60**, 024605 (1999).
 - [8] V.R. Pandharipande and R.B. Wiringa, *Rev. Mod. Phys.* **51**, 821 (1979).
 - [9] A. Akmal, V.R. Pandharipande, and D.G. Ravenhall, *Phys. Rev. C* **58**, 1804 (1998).
 - [10] A. Gezerlis *et al.*, *Phys. Rev. Lett.* **111**, 032501 (2013).
 - [11] G. Wlazłowski *et al.*, *Phys. Rev. Lett.* **113**, 182503 (2014).
 - [12] A. Roggero, A. Mukherjee, and F. Pederiva, *Phys. Rev. Lett.* **112**, 221103 (2014).
 - [13] K. Hebeler, J.M. Lattimer, C.J. Pethick, and A. Schwenk, *Phys. Rev. Lett.* **105**, 161102 (2010).
 - [14] I. Tews, T. Krüger, K. Hebeler, and A. Schwenk, *Phys. Rev. Lett.* **110**, 032504 (2013).
 - [15] M. Bender, P.-H. Heenen, and P.-G. Reinhard, *Rev. Mod. Phys.* **75**, 121 (2003).
 - [16] T. H. R. Skyrme, *Phil. Mag.* **1**, 1043 (1956).
 - [17] D. Vautherin and D. M. Brink, *Phys. Rev. C* **5**, 626 (1972).
 - [18] M. Dutra *et al.*, *Phys. Rev. C* **85**, 035201 (2012).
 - [19] J. Erler *et al.*, *Phys. Rev. C* **87**, 044320 (2013).
 - [20] W.C. Chen and J. Piekarewicz, *Phys. Rev. C* **90**, 044305 (2014).
 - [21] P.B. Demorest, T. Pennucci, S.M. Ransom, M.S.E. Roberts, and J.W.T. Hessels, *Nature (London)* **467**, 1081 (2010).
 - [22] J. Antoniadis *et al.*, *Science* **340**, 448 (2013).
 - [23] D.H. Youngblood, H.L. Clark, and Y.W. Lui, *Phys. Rev. Lett.* **82**, 691 (1999).
 - [24] T. Li *et al.*, *Phys. Rev. Lett.* **99**, 162503 (2007).
 - [25] D. Patel *et al.*, *Phys. Lett. B* **726**, 178 (2013).
 - [26] P. Danielewicz, R. Lacey, and W.G. Lynch, *Science* **298**, 1592 (2002).
 - [27] C. Fuchs, *Prog. Part. Nucl. Phys.* **56**, 1 (2006).
 - [28] J. Aichelin and C. M. Ko, *Phys. Rev. Lett.* **55**, 2661 (1985).
 - [29] D.W. Wen, B.A. Li, and L.W. Chen, *Phys. Rev. Lett.* **103**, 211102 (2009).
 - [30] M. I. Krivoruchenko, F. Simkovic, and A. Faessler, *Phys. Rev. D* **79**, 125023 (2009).
 - [31] D.R. Zhang, P.L. Yin, W. Wang, Q.C. Wang, and W.Z. Jiang, *Phys. Rev. D* **83**, 035801 (2011).
 - [32] H. Zheng and L.W. Chen, *Phys. Rev. D* **85**, 043013 (2012).
 - [33] C.J. Horowitz and J. Piekarewicz, *Phys. Rev. Lett.* **86**, 5647 (2001).
 - [34] R.J. Furnstahl, *Nucl. Phys. A* **706**, 85 (2002).
 - [35] N. Wang, L. Ou, and M. Liu, *Phys. Rev. C* **87**, 034327 (2013).
 - [36] P. Danielewicz and J. Lee, *Nucl. Phys. A* **922**, 1 (2014).
 - [37] Z. Zhang and L.W. Chen, *Phys. Lett. B* **726**, 234 (2013).
 - [38] B.A. Brown, *Phys. Rev. Lett.* **111**, 232502 (2013).
 - [39] Z. Zhang and L.W. Chen, *Phys. Rev. C* **92**, 031301(R), (2015).
 - [40] M.B. Tsang *et al.*, *Phys. Rev. Lett.* **102**, 122701 (2009).
 - [41] J. Margueron, J. Navarro and N. Van Giai, *Phys. Rev. C* **66**, 014303 (2002).
 - [42] I. Vidaña, A. Polls, and A. Ramos, *Phys. Rev. C* **65**, 035804 (2002); I. Vidaña and I. Bombaci, *Phys. Rev. C* **66**, 045801 (2002).
 - [43] F. Sammarruca and P.G. Krastev, *Phys. Rev. C* **75**, 034315 (2007).
 - [44] S. Fantoni, A. Sarsa, and K.E. Schmidt, *Phys. Rev. Lett.* **87**, 181101 (2001).
 - [45] F. Sammarruca, R. Machleidt, and N. Kaiser, *arXiv:1505.04836*.
 - [46] G.H. Bordbar and M. Bigdeli, *Phys. Rev. C* **77**, 015805 (2008).
 - [47] J. Margueron and H. Sagawa, *J. Phys. G* **36**, 125102 (2009).
 - [48] N. Chamel, S. Goriely and J.M. Pearson, *Phys. Rev. C* **80**, 065804 (2009).
 - [49] N. Chamel and S. Goriely, *Phys. Rev. C* **84**, 045804 (2010).
 - [50] M. Bender, J. Dobaczewski, J. Engel, and W. Nazarewicz, *Phys. Rev. C* **65**, 054322 (2002).
 - [51] S. Goriely, N. Chamel and J.M. Pearson, *Phys. Rev. C* **82**, 035804 (2010).
 - [52] S. Krewald, V. Klemt, J. Speth and A. Faessler, *Nucl. Phys. A* **281**, 166 (1977).
 - [53] L.X. Ge, Y. Z. Zhuo, and W. Norenberg, *Nucl. Phys. A* **459**, 77 (1986).
 - [54] Y.Z. Zhuo *et al.*, *Prog. Theor. Phys.* **79**, 110 (1988).
 - [55] S. Goriely, N. Chamel and J.M. Pearson, *Phys. Rev. C* **88**, 024308 (2013).
 - [56] S. Goriely, *Nucl. Phys. A* **933**, 68 (2015).
 - [57] E. Chabanat, P. Bonche, P. Haensel, J. Meyer and R. Schaeffer, *Nucl. Phys. A* **627**, 710 (1997).
 - [58] M. Waroquier *et al.*, *Phys. Rev. C* **19**, 1983 (1979).
 - [59] P. Ring and P. Shuck, *The Nuclear Many-Body Problems*, Springer, New York-Heidelberg-Berlin, 1980.
 - [60] L.W. Chen, B.J. Cai, C.M. Ko, B.A. Li, C. Shen, and J. Xu, *Phys. Rev. C* **80**, 014322 (2009).
 - [61] L.W. Chen, C.M. Ko, B.A. Li and J. Xu, *Phys. Rev. C* **82**, 024321 (2010).
 - [62] B.J. Cai and L.W. Chen, *arXiv:1402.4242*.
 - [63] B.K. Agrawal, S. Shlomo, and V.K. Au, *Phys. Rev. C* **72**, 014310 (2005).
 - [64] F. Osterfeld, *Rev. Mod. Phys.* **64**, 491 (1992).
 - [65] M. Baldo, U. Lombardo, E. E. Saperstein, and M. V. Zverev, *Phys. Lett. B* **421**, 8 (1998).
 - [66] W. Zuo, C.W. Shen, and U. Lombardo, *Phys. Rev. C* **67**, 037301 (2003).
 - [67] C.W. Shen, U. Lombardo, N. Van Giai, and W. Zuo, *Phys. Rev. C* **68**, 055802 (2003).
 - [68] T. Wakasa, M. Ichimura, and H. Sakai, *Phys. Rev. C* **72**, 067303 (2005).
 - [69] I. N. Borzov, *Nucl. Phys. A* **777**, 645 (2006).
 - [70] A. Bohr and B. Mottelson, *Nuclear Structure* (Benjamin, London, 1975), Vol. II.

- [71] O. Bohigas, A. M. Lane, and J. Martorell, Phys. Rep. **51**, 267 (1979).
- [72] T. Sil, S. Shlomo, B.K. Agrawal and P.-G. Reinhard, Phys. Rev. C **73**, 034316 (2006).
- [73] M. Wang *et al.*, Chin. Phys. C **36**, 1287 (2012).
- [74] I. Angeli, At. Data Nucl. Data. Tables **87**, 185 (2004).
- [75] F. Le Blanc *et al.*, Phys. Rev. C **72**, 034305 (2005).
- [76] Z. Zhang and L.W. Chen, Phys. Rev. C **90**, 064317 (2014).
- [77] Z. Zhang and L.W. Chen, arXiv:1507.04675.
- [78] C. Xu, B.A. Li, and L.W. Chen, Phys. Rev. C **82**, 054607 (2010).
- [79] X.H. Li, W.J. Guo, B.A. Li, L.W. Chen, F.J. Fattoyev and W.G. Newton, Phys. Lett. **B743**, 408 (2015).
- [80] R. Klüpfel, P.-G. Reinhard, T.J. Bürvenich and J.A. Maruhn, Phys. Rev. C **79**, 034310 (2009).
- [81] B. A. Brown, Phys. Rev. Lett. **85**, 5296 (2000).
- [82] S. Typel and B. A. Brown, Phys. Rev. C **64**, 027302 (2001).
- [83] L.W. Chen, C. M. Ko, and B.-A. Li, Phys. Rev. C **72**, 064309 (2005).
- [84] X. Roca-Maza *et al.*, Phys. Rev. C **88**, 024316 (2013).
- [85] C.M. Tarbert *et al.*, Phys. Rev. Lett. **112**, 242502 (2014).
- [86] S. Abrahamyan *et al.*, Phys. Rev. Lett. **108**, 112502 (2012).
- [87] M. Bender, W. Nazarewicz and P.-G. Reinhard, Phys. Lett. **B515**, 42 (2001).
- [88] B.M. Tsang *et al.*, Phys. Rev. C **86**, 015803 (2012).
- [89] J.M. Lattimer, Ann. Rev. Nucl. Part. Sci. **62**, 485 (2012).
- [90] L.W. Chen, in Nuclear Structure in China (2012), *Proceedings of the 14th National Conference on Nuclear Structure in China (NSC2012)*, Hu-Zhou, Zhejiang, China, 2012, edited by J.Meng, C.-W. Shen, E.-G. Zhao, and S.-H. Zhou (World Scientific, Singapore, 2012), pp. 43 - 54 [arXiv:1212.0284].
- [91] B.A. Li *et al.*, J. Phys.: Conf. Series **413**, 012021 (2013) [arXiv:1212.1178].
- [92] L.W. Chen, EPJ Web of Conf. **88**, 00017 (2015) [arXiv:1506.09057].
- [93] Z.H. Li and H.-J. Schulze, Phys. Rev. C **78**, 028801 (2008).
- [94] E. Suraud, C. Gregoire, and B. Tamain, Prog. Part. Nucl. Phys. **23**, 357 (1989).
- [95] F.S. Zhang and E. Suraud, Phys. Rev. C **51**, 3201 (1995).
- [96] R.C. Tolman, Phys. Rev. **55**, 364 (1939).
- [97] J.R. Oppenheimer and G.M. Volkoff, Phys. Rev. **55**, 374 (1939).
- [98] G. Baym, C.J. Pethick, and P. Sutherland, Astrophys. J. **170**, 299 (1971).
- [99] J. Carrier, C.J. Horowitz and J. Piekarewicz, Astrophys. J. **593**, 463 (2003).
- [100] J. Xu, L. W. Chen, B. A. Li, and H. R. Ma, Phys. Rev. C **79**, 035802 (2009); Astrophys. J. **697**, 1549 (2009).
- [101] A.W. Steiner, J.M. Lattimer, and E.F. Brown, Astrophys. J. **722**, 33 (2010).
- [102] V. Suleimanov, J. Poutanen, M. Revnivtsev, and K. Werner, Astrophys. J. **742**, 122 (2011).
- [103] S. Guillot, M. Servillat, N. A. Webb, and R. E. Rutledge, Astrophys. J. **772**, 7 (2013).
- [104] J.M. Lattimer and A.W. Steiner, Astrophys. J. **784**, 123 (2014).
- [105] J.M. Lattimer and M. Prakash, Astrophys. J. **550**, 426 (2001).